# Monitoring seasonal deformation behavior of an immersed tunnel with distributed optical fiber sensors

Zhang, Xuehui; Broere, Wout

**DOI**
10.1016/j.measurement.2023.113268

**Publication date**
2023

**Document Version**
Final published version

**Published in**
Measurement: Journal of the International Measurement Confederation

**Citation (APA)**
Zhang, X., & Broere, W. (2023). Monitoring seasonal deformation behavior of an immersed tunnel with distributed optical fiber sensors. *Measurement: Journal of the International Measurement Confederation*, *219*, Article 113268. https://doi.org/10.1016/j.measurement.2023.113268

Measurement 219 (2023) 113268

Contents lists available at ScienceDirect

Measurement

journal homepage: www.elsevier.com/locate/measurement

# Monitoring seasonal deformation behavior of an immersed tunnel with distributed optical fiber sensors

Xuehui Zhang , Wout Broere *

*Geo-Engineering Section, Department of Geoscience and Engineering, Delft University of Technology, Delft, the Netherlands*

ARTICLE INFO

*Keywords:*
Immersed tunnel
Joint deformation
Distributed optical fiber sensor (DOFS)
Seasonal deformation
Tunnel safety

ABSTRACT

Seasonal joint deformations within an immersed tunnel are important indicators to assess structural behavior and therefore should be monitored in detail. In this study, distributed optical fiber sensors (DOFS) are applied to precisely measure the seasonal joint deformations in an immersed tunnel for the first time. Measurements over a one-year period specifically reveal the impact of seasonal temperature variations on the joint opening and uneven settlement deformation. Field monitoring shows that the variation in joint opening exhibits a cyclic behavior and is strongly correlated with temperature change. The immersion joints generally show a larger range of seasonal opening (with a maximum of about 6 mm) than dilation joints, but at several dilation joints significant opening also occurs. The uneven or differential settlement at most joints stays below 1 mm, except at a few joints where the range is above 1 mm, which are indications of underlying structural defects in the tunnel. The observed joint uneven settlement also shows a seasonal variation, but the correlation with temperature is weak. The impacts of seasonal deformation on the structural integrity and watertightness of the tunnel are assessed, and further suggestions on tunnel maintenance and inspection are made.

## 1. Introduction

Immersed tunnels are mostly constructed and used as fixed links under waterways, where they possess advantages over a bridge or a bored tunnel. When constructing an immersed tunnel, a series of segments are prefabricated and joined into several elements, which are subsequently immersed and connected underwater along the designated alignment. Generally, two types of structural joints, namely immersion joints (between elements) and dilation joints (between the individual segments), are formed in this process. Since the first immersed tunnel for traffic use, the Detroit River Tunnel, was built in 1910, there have been more than 150 immersed tunnels built worldwide that are still in service, and about one-third of these have an over-50-year service period [7]. With more and more immersed tunnels exceeding half of their designed lifespan, monitoring their structural health conditions has increasingly become an essential task in immersed tunnel maintenance.

There are signs of structural deterioration observed in immersed tunnels, which include excessive uneven settlements, leakages at structure joints, and local concrete cracking, among others [5,11,21]. It should be mentioned that even some relatively young immersed tunnels, with a service time of only 20–30 years, also show structural deterioration already [2,9,23]. The observed signs of structural deterioration, especially where it concerns local damage and leakages, strongly imply that more emphasis shall be put on the structural health monitoring of existing immersed tunnels [3].

The deformation behavior of immersed tunnels under seasonal temperature variation affects structural safety, and forms an important indicator in tunnel structural health monitoring. For example, at the Kiltunnel in the Netherlands the seasonal deformation at the joints is supposed to cause decompression of the rubber gasket seals and impose a subsequent leakage risk [1,21]; in the Shanghai Outer-ring Expressway Tunnel, it is deduced that the seasonal temperature variation causes a possible cyclic opening deformation at joints which is related to the damage of the rubber gasket seal [2]. Therefore, it is necessary to quantify the seasonal deformation through actual field monitoring, as well as to further assess its impact on structural safety and operation of the tunnel.

However, currently there are hardly any studies on the seasonal deformation behaviour and its magnitude based on actual field monitoring of the entire joints (either dilation or immersion joints) within an immersed tunnel. For example, in most older immersed tunnels in the Netherlands, the joint deformations (opening and uneven settlement)

* Corresponding author at: Delft University of Technology, Stevinweg 1, 2628 CN Delft, the Netherlands.
*E-mail address:* W.Broere@tudelft.nl (W. Broere).

https://doi.org/10.1016/j.measurement.2023.113268
Received 25 January 2023; Received in revised form 14 June 2023; Accepted 29 June 2023
Available online 30 June 2023

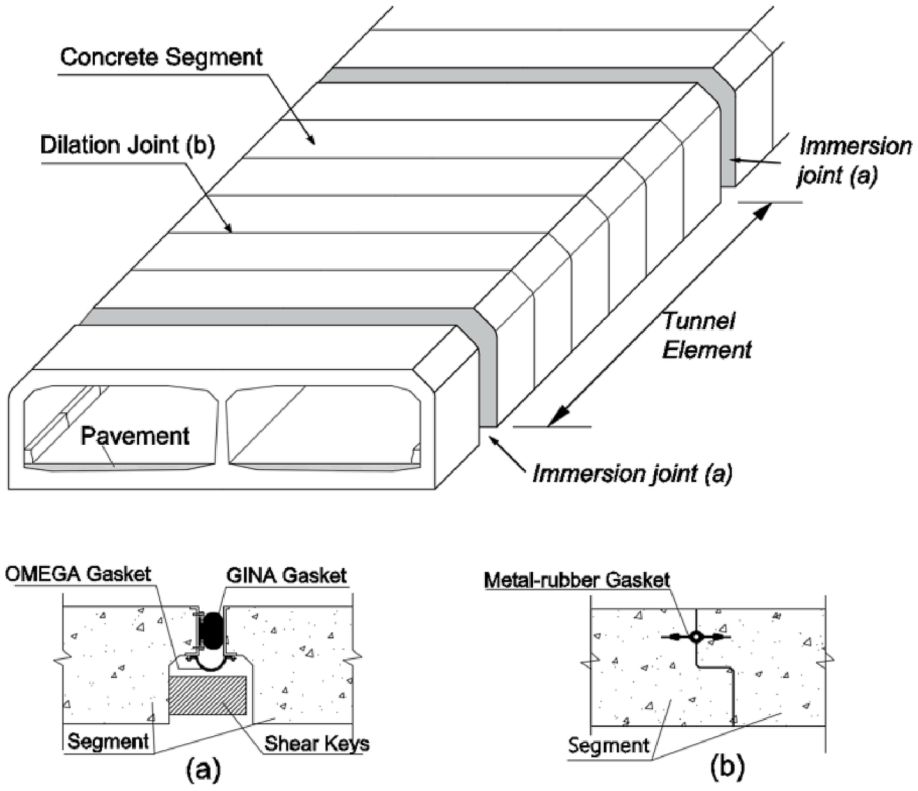


**Fig. 1.** Segmented immersed tunnel and joint: (a)immersion joint and (b)dilation joint.

are rarely monitored [1,21]. An important reason underlying this lack of monitoring, is a lack of qualified sensing techniques that can conveniently instrument a large number of monitoring points (i.e, all the joints) economically, whilst generating precise daily or weekly measurements and imposing limited interference with regular tunnel operation.

Distributed optical fiber sensor (DOFS) is a type of sensing technology that features distributed strain and temperature measurements. A DOFS system generally consists of an optical fiber cable (also known as a sensing fiber) and a signal interrogator, with the optical fiber attached to the structure and the interrogator measuring the spatial-resolved strain or temperature along the fiber axis [8,6,15]. DOFS provides several advantages over conventional electronic sensors, including distributed sensing, long sensing distances of up to a hundred kilometers and immunity to electromagnetic interferences [12]. In previous studies, DOFS has been explored to monitor deformations in, amongst other, bored tunnels [13,22,20,24], and pipelines [10]. Given the advantages of both distributed and long-distance sensing, DOFS offers a great potential to set up a monitoring system to observe seasonal deformations in immersed tunnels, and investigate the impacts on structural safety. However, so far there has been little use of DOFS for monitoring immersed tunnels, and large knowledge gaps still exist about the practical setup of such monitoring systems, as well as for the subsequent assessment of tunnel structural safety. The present study addresses these gaps.

In this study, a distributed optical fiber sensor (DOFS) system is firstly designed and successfully implemented to monitor an immersed tunnel structure, the First Heinenoordtunnel in the Netherlands. This DOFS system proves capable of measuring both immersion and dilation joint deformations (joint opening and uneven settlement). The field monitoring during a one-year period reveals the seasonal behavior of the immersed tunnel. In the rest of the paper, firstly some background information on the immersed tunnel joint deformations and the necessity of monitoring are described; secondly, the DOFS technique is introduced, followed by a demonstration of the monitoring system design and field instrumentation; thirdly, the observed joint deformation behavior within the one-year period is investigated; finally, the impacts of seasonal joint deformation on structure safety are assessed, and suggestions on future tunnel maintenance work are put forward.

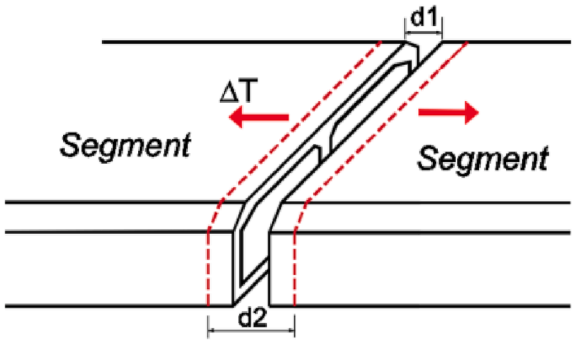


**Fig. 2.** Longitudinal segment expansion and resultant joint opening variation.

### 1.1. Seasonal joint deformation in immersed tunnels

An immersed tunnel structure generally consists of a series of prefabricated elements that are immersed and connected underwater, as depicted in Fig. 1. Within a segmented immersed tunnel, two different types of joints, namely immersion and dilation joints, are formed in the construction process [7].

Immersion joints are formed when a new element is immersed and connected to the finished one or the end approach structure under the water. A typical immersion joint uses a GINA gasket installed circumferentially as an initial seal at the construction stage, while an OMEGA gasket is installed internally as a secondary seal, as shown in Fig. 1(a). Although the GINA gasket is designed only to function in the initial

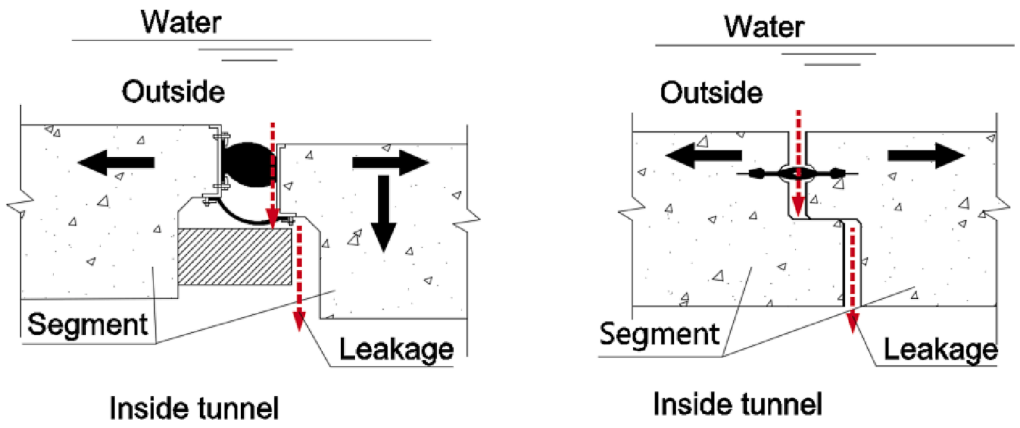


**Fig. 3.** Potential joint deformation patterns under seasonal temperature variation (left as immersion joint and right as dilation joint).

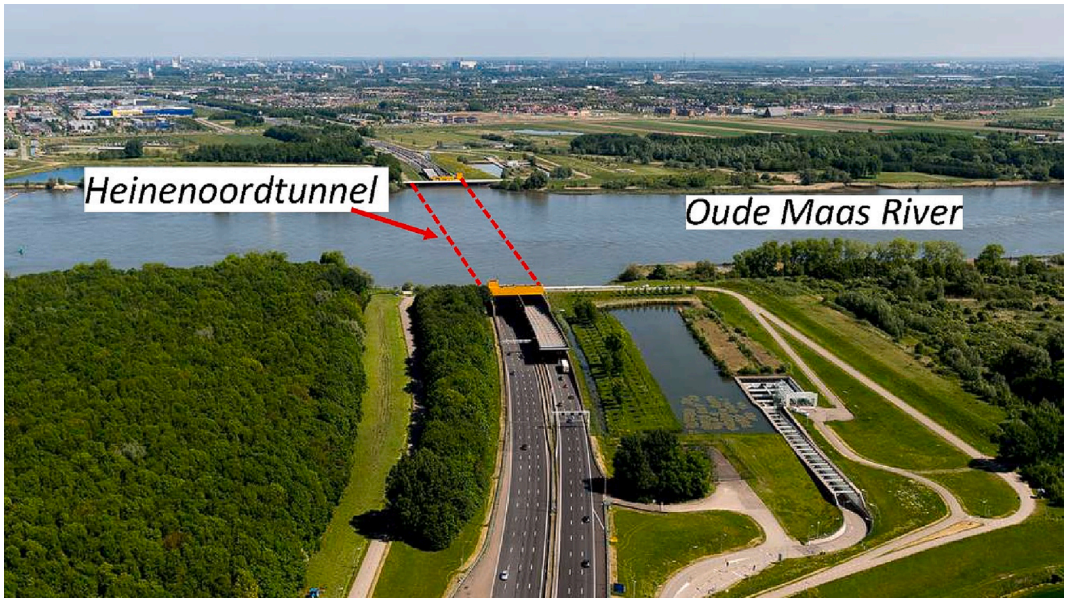


**Fig. 4.** The First Heinenoordtunnel under the Oude Maas River (from [18].

construction period, its sealing performance actually still decides the joint watertightness during the extended service period. Moreover, a cast-in-situ shear key is constructed to provide shear resistance in the vertical direction. Dilation joints are formed when the long elements are divided into several shorter segments in a dry dock. At the dilation joints, a concrete-concrete interface is formed and an embedded metal-rubber gasket is used for joint sealing, as shown in Fig. 1(b).

The seasonal temperature variation causes thermal expansion and contraction of tunnel segment bodies in the longitudinal direction (see Fig. 2), which further causes seasonal cyclic joint (gap) opening [28] as shown in Fig. 3. These joint openings decompress (or relax) the rubber seals at the joints and affect their sealing performance. In addition, joint opening indicates the interface contact status, and further affects the friction resistance to the concentrated shear deformation at the joint along vertical direction (see Fig. 3(a)). The seasonal joint deformations are associated with some widely observed safety issues in immersed tunnels, such as joint leakage[21], local concrete cracking [5] and damage of gasket seals [2], and therefore to quantify these joint

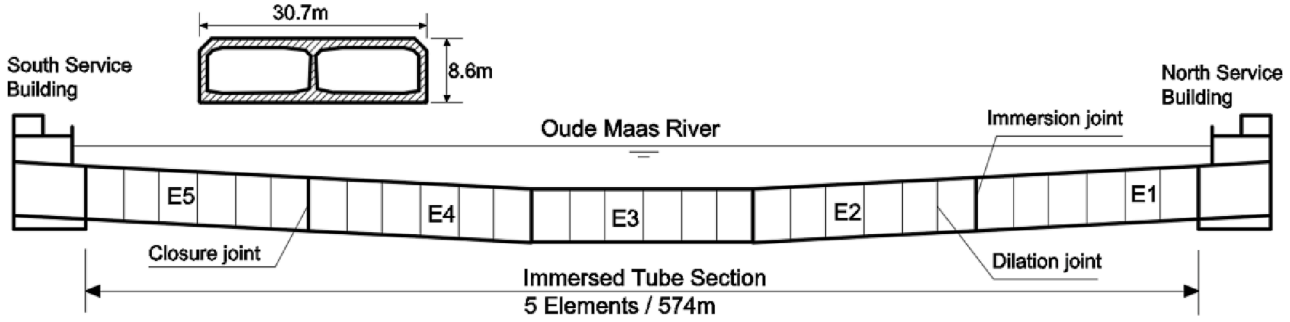


**Fig. 5.** Side view of the First Heinenoordtunnel.

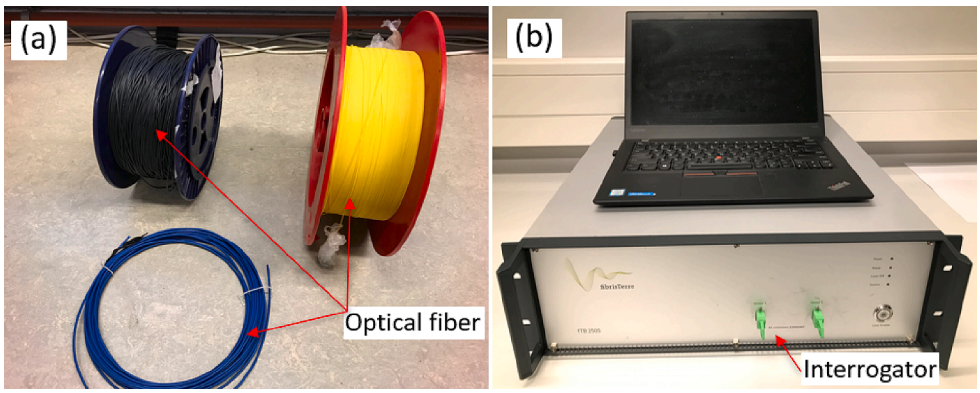


**Fig. 6.** Schematic of the DOFS system: (a) optical fiber and (b) interrogator.

deformations via actual field monitoring helps the tunnel manager to better assess the impacts of seasonal temperature variation on tunnel safety.

### 1.2. The first Heinenoordtunnel

In this study, the First Heinenoordtunnel (hereafter Heinenoordtunnel for brevity) in the Netherlands is selected to be instrumented with DOFS for seasonal deformation observation. The Heinenoordtunnel is a segmented immersed tunnel constructed under the Oude Maas River, see Fig. 4. This tunnel has a rectangular concrete cross-section (30.7 m wide and 8.6 m high) and was opened in 1969. The total length of the immersed tube section is 574 m, and composed of 5 concrete elements longitudinally, each measuring about 115 m long, whilst each element is further divided into 6 segments of about 19 m in length individually. In the Heinenoordtunnel there are 31 joints in total, including 25 dilation joints and 6 immersion joints as depicted in Fig. 5. The immersion joints and dilation joints in the Heinenoordtunnel have a typical design as shown in Fig. 1(a) and 1(b).

After over 50 years of service period, the structural integrity of the Heinenoordtunnel has become a safety issue and significant deformation has been observed. At two locations coinciding with dilation joints, water leakages and concrete cracking have been observed, which implies excess joint opening or compression may have occurred; at several immersion joint, uneven settlement was observed to further triggers a twisting deformation of the OMEGA gasket, and the water pit in the joint gap may possibly imply the occurrence of leakage. Seasonal temperature loading may have a negative impact on structural safety, according to observations from similar immersed tunnels and indoor experiments, but the Heinenoordtunnel lacks field measurements that can definitively verify this behavior, and a yearly or multi-year monitoring interval will not reveal such seasonal influences [19].

In this study, the DOFS is designed to build a monitoring system which instruments the entire joints of the Heinenoordtunnel (see Fig. 4), for measuring the seasonal joint deformations along two directions, namely the horizontal joint opening and the vertical uneven settlement (between the two sides of the joint), as demonstrated in Fig. 2.

## 2. DOFS based monitoring system design and field instrumentation

### 2.1. Distributed optical fiber sensor (DOFS)

This study utilized the DOFS based on Brillouin scattering phenomenon inside an optical fiber. In brief, Brillouin scattering triggers a frequency shift between the Brillouin backscattered light and the original propagating light [8]. This Brillouin frequency shift (BFS) $\Delta\nu$ has a linear relation to the fiber strain ($\varepsilon$) and temperature variation ($\Delta T$) [15,12], as shown in Eq.1:

$$\Delta\nu = C_\varepsilon\varepsilon + C_t\Delta T \tag{1}$$

where $C_\varepsilon$ and $C_t$ are strain and temperature sensitivity coefficients of the optical fiber. By independently measuring the local temperature variation, preferably using a zero-strain parallel fiber section, the temperature component $C_t\Delta T$, can be compensated for, and the strain distribution along the optical fiber can be determined.

A complete DOFS system is composed of a long optical fiber (sensing fiber) that is extended and attached to the monitored structure properly, and a terminal signal interrogator for data-taking (including data-taking software), as shown in Fig. 5. There are different available (Brillouin scattering) interrogators that differ in the precise method used to measure the BFS, resulting in differences in spatial accuracy and attainable measurement frequency [8,12]. In this study a Brillouin Optic Frequency Domain Analyzer (BOFDA) interrogator is used, which has high spatial accuracy but requires the sensing fiber to form an entire loop with both ends plugged into the interrogator.

### 2.2. DOFS based monitoring system design

When conducting deformation monitoring using DOFS, the optical

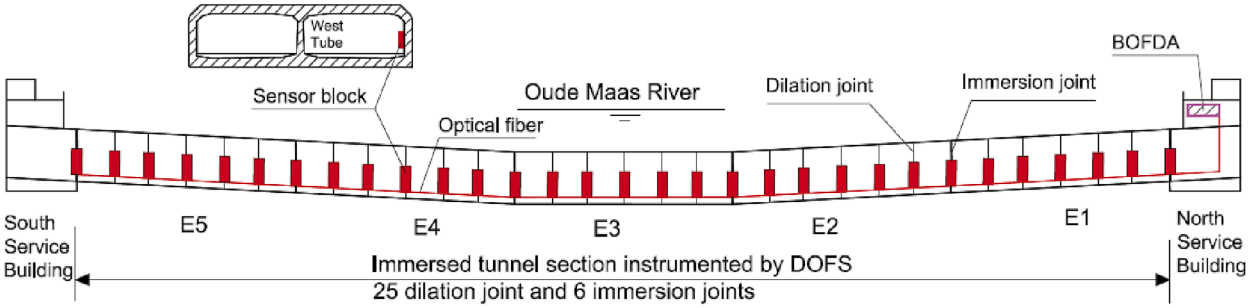


**Fig. 7.** Field DOFS monitoring system configuration in Heinenoordtunnel.

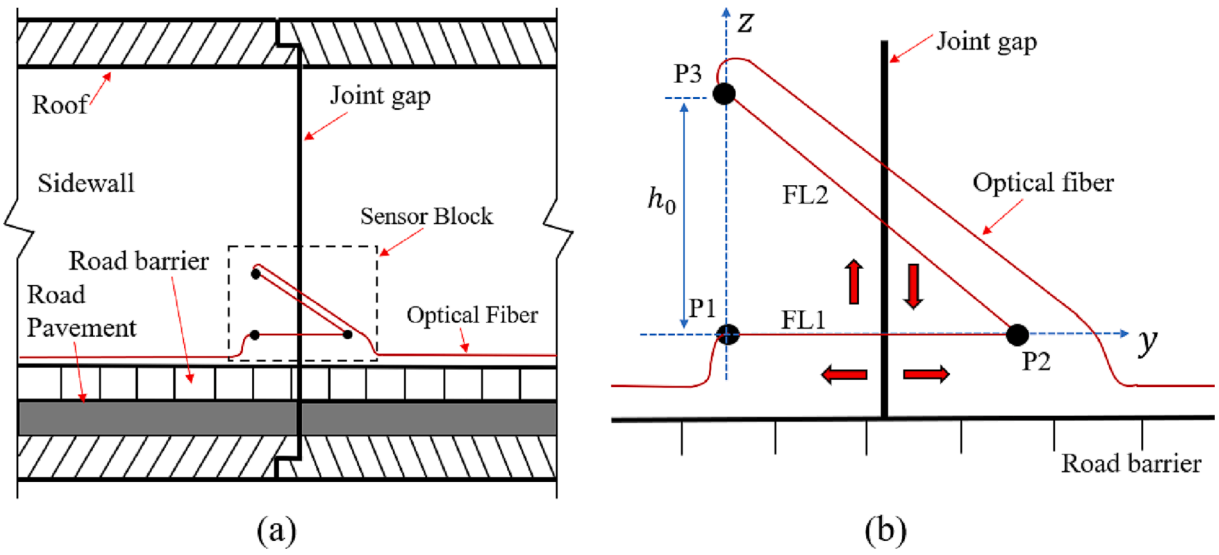


**Fig. 8.** Sensor block design at joint for two-directional displacement measuring: (a) sensor layout in tunnel and (b) sensor details.

fiber should be attached to the host structure properly, such as by bonding on surface or being embedded inside material for distributed strain sensing [20,25], while one or both of the fiber ends are plugged to the interrogator for signal processing and data-taking.

However, for immersed tunnel monitoring in this study, the DOFS is designed to monitor the localized displacements (or deformations) at specific joint locations along the tunnel, rather than the distributed strain along the tunnel segment bodies. As the Heinenoordtunnel is chosen for field monitoring implementation, the DOFS monitoring system installed should not interfere with the traffic in the tunnel. Moreover, there is no storage space in this tunnel, thus the interrogator system must be placed outside of it. Therefore, a suitable field monitoring configuration should be that: a long optical fiber cable extends longitudinally along the tunnel axis and is installed as a special sensor block at each joint for deformation sensing (joint opening and uneven settlement), while the fiber ends extend further outside the tunnel to the interrogator, as depicted in Fig. 7.

For the sensor block design at an individual joint, the fiber should be installed in such a layout that the strain information captures both the joint opening and uneven settlement. This monitoring goal is achieved by the sensor layout illustrated in Fig. 8. At each joint, two short fiber lengths are fixed at three points, indicated as fixation points P1 to P3 in Fig. 8(b). The two strained fiber lengths (FL1 and FL2) and three fixation points combine to form a sensor block that detects the joint deformations in two directions (opening along Y-axis and uneven settlement along Z-axis). The mathematical equations for strain-joint deformation transfer are derived in the following section.

When a certain displacement in both horizontal and vertical directions occurs at the joint, FL1 will detect only the horizontal component, which simplification is reasonable as the influence of any vertical component on the FL1 strain is insignificant. At time interval $i$, the relation between fiber strain and deformation for FL1 can be expressed as:

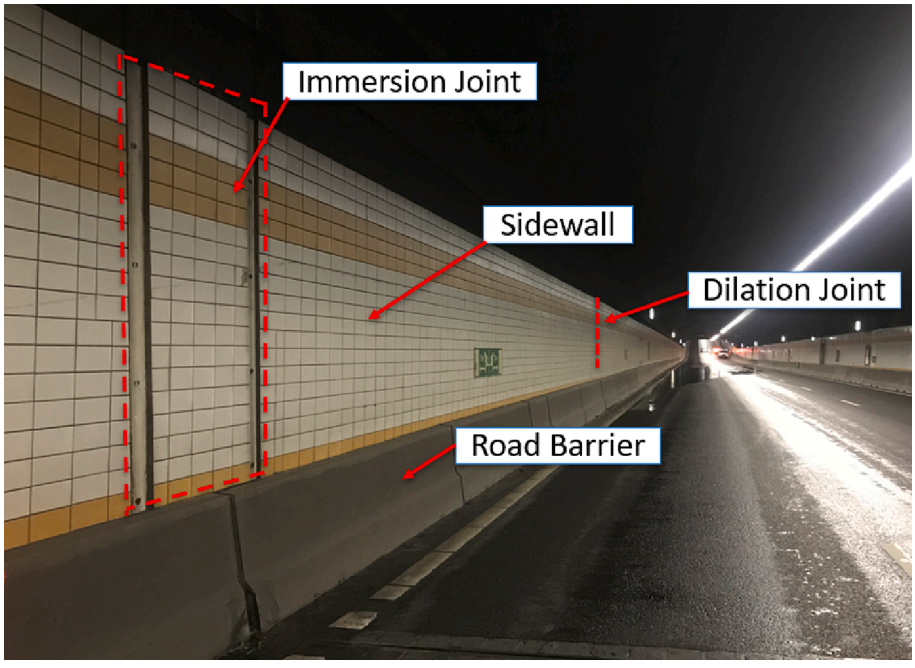


**Fig. 9.** Heinenoordtunnel joints to be instrumented by DOFS (west tube).

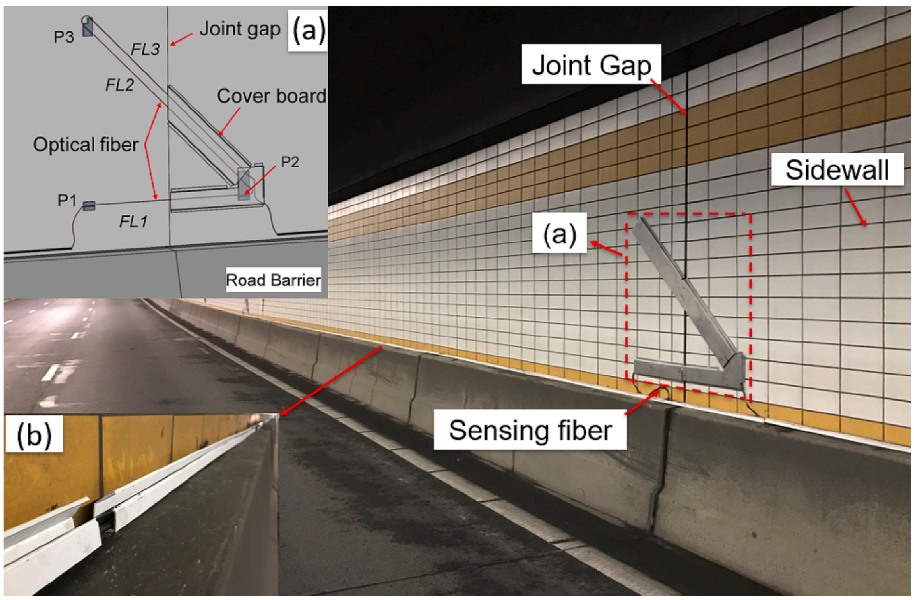


**Fig. 10.** Field fiber sensor installation in the Heinenoordtunnel:(a) Sensor layout at joint;(b) Loose fiber cable in PVC duct.

$$\varepsilon_{1,i} = \frac{\Delta\nu_{1,i}}{c_\varepsilon} \tag{2}$$

$$l_{1,i} = l_1(1+\varepsilon_{1,i}) \tag{3}$$

$$\Delta y_i = l_1\varepsilon_{1,i} \tag{4}$$

For FL2, it follows that:

$$\varepsilon_{2,i} = \frac{\Delta\nu_{2,i}}{c_\varepsilon} \tag{5}$$

$$l_{2,i} = l_2\left(1+\varepsilon_{2,i}\right) \tag{6}$$

And the height difference between FP1 and FP3 is calculated by:

$$h_i = \sqrt[2]{l_{2,i}^2 - l_{1,i}^2} \tag{7}$$

where $l_{1,i}/l_{2,i}$ are the lengths of FL1/FL2 at interval $i$; $\Delta\nu_{1,i}/\Delta\nu_{2,i}$ are the Brillouin frequency shifts of FL1/FL2 at interval $i$ (with temperature effects deducted) measured by the interrogator; $\varepsilon_{1,i}/\varepsilon_{2,i}$ are the strains of FL1/FL2 at interval $i$; $\Delta y_i$ is the extension of FL1 at interval $i$; and $h_i$ is the height difference between fixation points FP1 and FP3.

For a measurement at the same joint at a later time interval $j$, the displacement–strain relations remain the same as in Eq. (2) to Eq. (7), and the joint deformation relative to interval $i$ can be obtained as:

$$\Delta y = \Delta y_j - \Delta y_i \tag{8}$$

$$\Delta z = h_j - h_i \tag{9}$$

In addition, an experimental study has been conducted by Zhang and Broere [27] to validate the performance and potential error sources of the designed sensor block (shown in Fig. 8) for two-directional joint deformation monitoring. The laboratory experiment has verified the designed sensor can effectively capture two-directional joint deformations with sub-millimeter precision; a maximum relative error of only 6% was reported for joint opening, and less than 10% for joint uneven settlement. In summary, the developed sensor layout demonstrates a sufficient level of accuracy and performance for subsequent field monitoring.

**Table 1**
Sensor block parameters as used in field installation.

| Parameter | Immersion joint | Dilation joint |
|---|---|---|
| FL1 | 1350 mm | 800 mm |
| FL2 | 1902 mm | 1127 mm |
| $h_0$ | 1350 mm | 800 mm |

### 2.3. Field sensor installation and data-taking

For field monitoring in the Heinenoordtunnel, only the sidewall in the west tube is accessible for sensor instrumentation, see Fig. 9. A polyurethane sheath fiber type NZS-DSS-C07 with a diameter of 2 mm was chosen as the sensing fiber. This optical fiber type, manufactured by Nanzee Sensing Company, has a strain sensitivity of 48.55 MHz/0.1% and a maximum working strain of above 1.2% [26].

Fig. 10 schematically shows the installed sensor in the Heinenoordtunnel. To reduce the difficulty of sensor installation in the field, the optical fiber is first bonded to small fixation pads at designated locations, see P1 to P3 in Fig. 10(a), and then these three pads are mounted on the sidewall at precise distances in subsequent fieldwork. Moreover, the bare sensing fiber crossing the joint is protected (from potential external impacts) by special cover boards made of thin steel plate, as illustrated in Fig. 10(a). It should be pointed out that fiber line 3 (FL3) in Fig. 10(a) is unstrained and aligned parallel to FL2 just for the convenience of fiber protection. The field sensor's parameters (gauge length and dimensions) are depicted in Fig. 8 and specified in Table 1.

The optical fiber sensor forms a loop with a total length of about 1.4 km, and both fiber ends are extended on the barrier top (see Fig. 10(b)) until the outside the tunnel at the North portal and connected to the BOFDA interrogator located in the service building. This BOFDA interrogator, type fTB2505 and manufactured by fibrisTerre Systems GmbH, has a stated spatial resolution of 0.2 m (up to 2 km) and fiber strain accuracy of 2 micro-strain (0.0002%), according to fibrisTerre [4]. The DOFS monitoring system realized in this manner can be remote-controlled and proves to have no disturbance to traffic in the tunnel.

The monitoring periods of the individual joints are:

(1). The first set of thirteen joints (within the two elements E1 and E2, see Fig. 5) were instrumented at the first stage of the fieldwork,

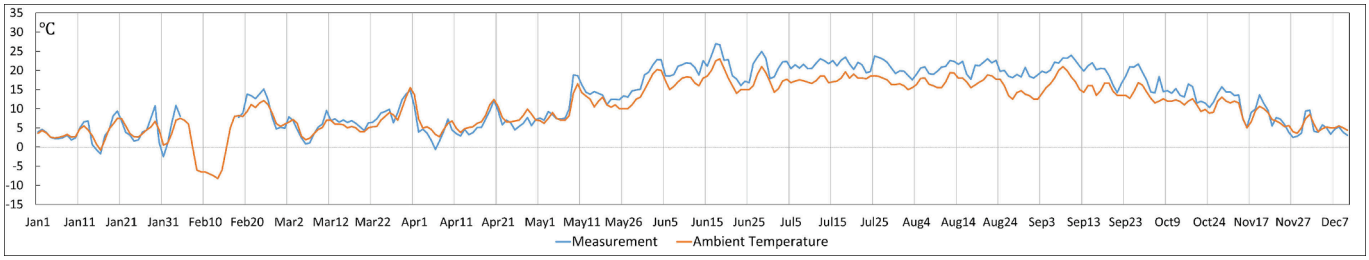


**Fig. 11.** Comparison between temperature measurement and ambient air temperature.

with a full-year monitoring duration. The data acquisition started on December 16, 2020, until December 11, 2021;

(2). The second set of seventeen joints (within the three elements within the three elements E3, E4 and E5, see Fig. 5) were instrumented at the second stage of fieldwork, with a half-year monitoring duration. The data acquisition started on June 11, 2020, until to December 11, 2021. Note the second dilation joints within the fifth element was not instrumented due to working space limitation;

The field monitoring covers a long period from summer to winter, and the monitoring results can help to interpret the seasonal behavior of the Heinenoordtunnel.

### 2.4. Performance of DOFS monitoring system in field conditions

The measurement accuracy of the DOFS monitoring system for a one-year period in field conditions shall be assessed firstly. Here the system accuracy is evaluated with regard to two aspects: (1) a comparison of temperature measurements with ambient weather temperature; and (2) the optical fiber signal attenuation check.

As an initial verification of the DOFS system, the measured temperature of the most northern joint (the first immersion joint from the north portal of Heinenoordtunnel) is compared with the outside ambient temperature (daily mean, from Meteoblue [14]) as recorded by a nearby meteorological station in the Heinenoord area. The BFS of the unstrained fiber section at reference temperature ($T_0$ = 22.8 °C) was determined before field installation, and the temperature measured at each joint in Heinenoordtunnel can be calculated from Eq. (10):

$$T = T_0 + \left(\nu_{t,i} - \nu_{t,0}\right)/C_t \tag{10}$$

where $C_t$ is the temperature sensitivity coefficient of the optical fiber (1.89 Mhz/°C), $\nu_{t,0}$ indicates the BFS at reference temperature $T_0$; $\nu_{t,i}$ is the measured BFS at time interval $i$.

The measured temperature results are plotted in Fig. 11, and it can be seen that the measurements closely follows the ambient weather temperature throughout the monitoring period. Considering that the weather station in Heinenoord is located approximately 3 km from the north tunnel portal, a slight temperature difference between them is reasonable. In summary, the temperature monitoring results by the DOFS sensor in field conditions are reliable.

A further factor that influences the measurement reliability is the signal attenuation in the optical fiber loop. This signal attenuation is generally related to the fiber length, the quality of connector and splice and local fiber bends. According to Fibristerre [4], depending on the local distribution of the attenuation sources, a total attenuation of below 6 dB are desirable in order to get reliable and reproducible results. The BOFDA interrogator can detect signal attenuation and adjust the output power automatically to get optimal results. Before field installation, the 1.4 km optical fiber loop has a signal attenuation of below 1.5 dB, and in the field working conditions the measured signal attenuation is about 3 dB, which indicates a limited attenuation level. Therefore, it is reasonable to conclude the installed DOFS monitoring system has an acceptable accuracy in field conditions.

## 3. Seasonal deformation monitoring result

The instrumented tunnel joints are numbered for easy identification: *Ij* denotes the *j th* immersion joint from the north end (see Fig. 12), while *Dik* refers to the *kth* dilation joint (from north) in the *ith* element. For example, I1 refers to the first immersion joint, while D21 means the first dilation joint (from north) in the second element. Note that the second dilation joint in the 5th element (i.e. D52) was not instrumented due to working space limitations.

### 3.1. Temperature results

Here for brevity, only the measured temperature (daily mean) of the immersion joints is presented, which helps to show the temperature variation along the tunnel axis longitudinally.

Fig. 13 shows the measured temperature of joints I1 to I3 within one

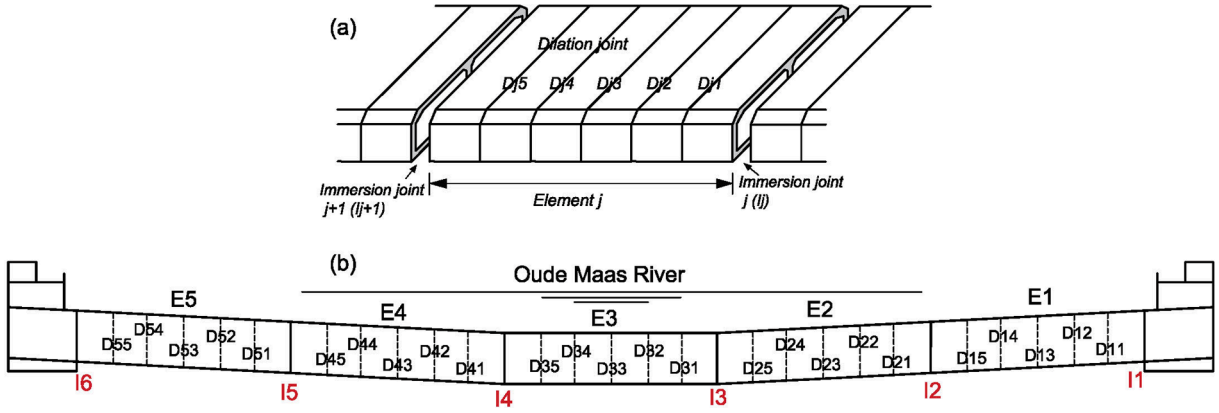


**Fig. 12.** Tunnel joint numbering (a) within an element and (b) along tunnel longitudinal axis.

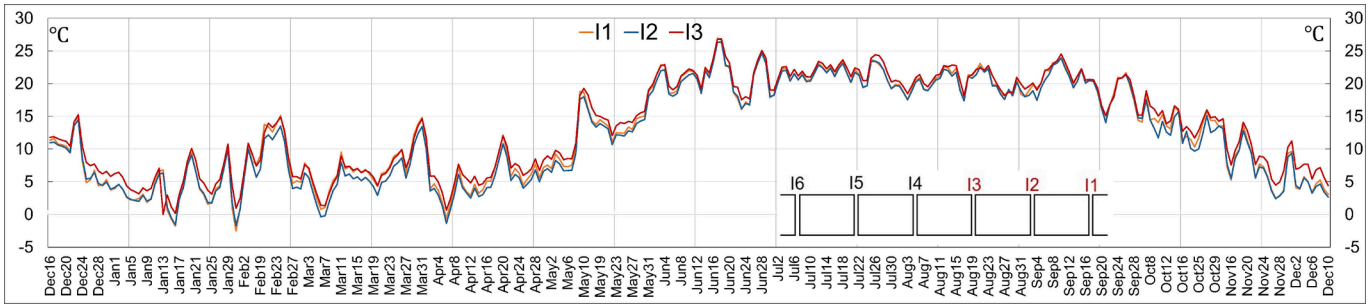


**Fig. 13.** The measured temperature of immersion joint (I4 to I6, half-year period).

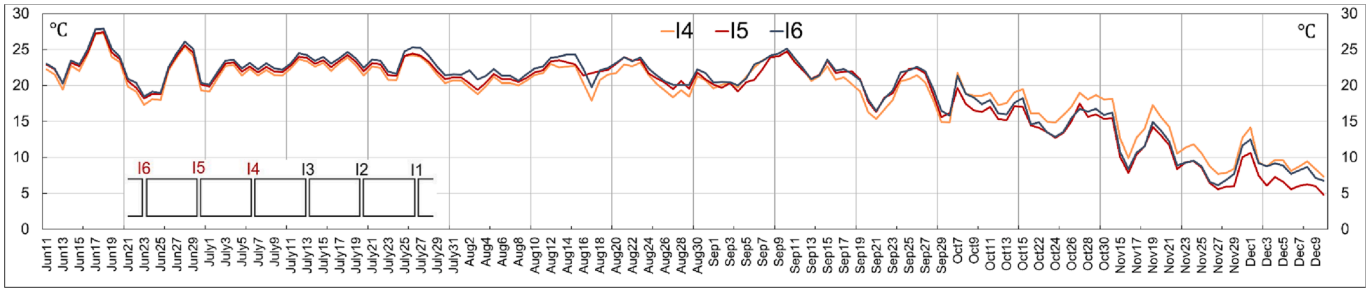


**Fig. 14.** The measured temperature of immersion joint (I1 to I3, full-year period).

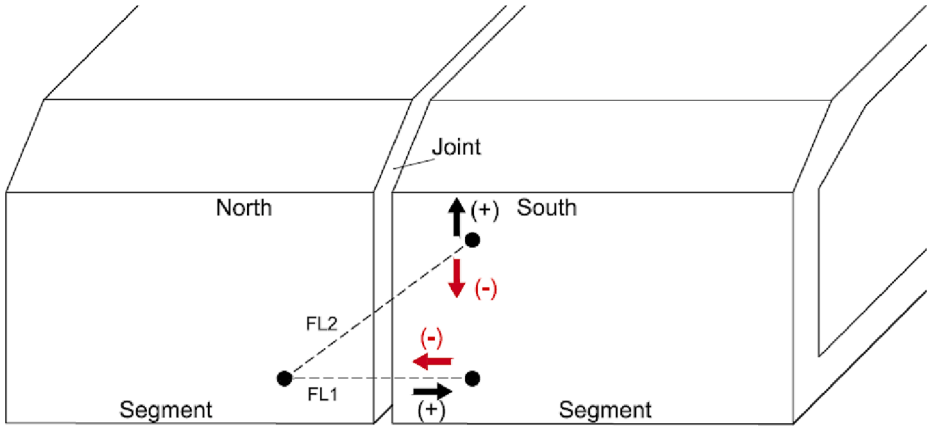


**Fig. 15.** Joint deformation mode analysis (not to scale, viewed from outside tunnel).

year. The DOFS system accurately measures the seasonal temperature variation, as shown in the temperature curves. It can be noticed that the temperatures of the three immersion joints are very close, with a maximum difference of about 3 °C. According to the measurements, the seasonal temperature fluctuation (absolute value) inside the Heinenoordtunnel over the monitoring period is about 30 °C.

Fig. 14 shows the temperature results of joints I4 to I6 within a half-year period. As seen in the temperature curves, the measured

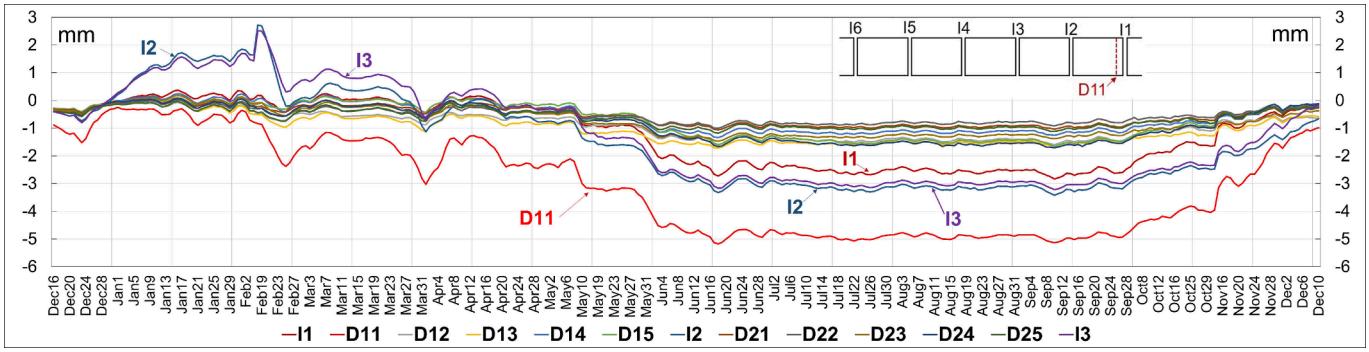


**Fig. 16.** The measured opening of first-set 13 joints (full-year period).

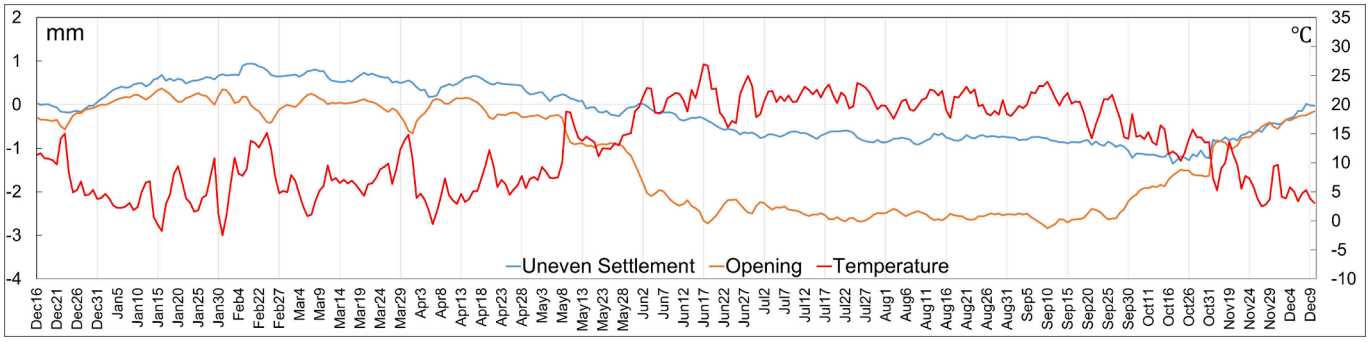


**Fig. 17.** Joint deformation and temperature of immersion joint I1.

temperatures of the three immersion joints are again close, with the highest difference of around 4.5 °C From June 11 to December 10, the amplitude of temperature fluctuation is about 23 °C Observing the temperature curves on the overlapping period (June 11 to December 10) in Figs. 13 and 14, the measured temperatures at the six immersion joints are very close and share a highly similar tendency, while the differences between them are very small (below 4.5℃), which indicates that the environmental temperature varies a limited amount along the tunnel axis longitudinally.

### 3.2. Joint deformation behavior monitoring results

As shown in Fig. 15, for joint opening negative values indicate the fiber get shorter and hence the joint closes compared to the baseline status (the first measurement on December 11, 2020), while a positive value shows joint opening. For joint uneven or differential settlement, if the north side (of the joint) is assumed static, a positive settlement value indicates the south side moves upwards, while a negative value indicates a downward settlement.

#### 3.2.1. Joint opening

Positive joint opening denotes a joint gap widening compared to the baseline status, whereas a negative opening indicates a joint gap closure. Fig. 16 depicts the joint opening of the first thirteen joints (from I1 to I3) during the entire year period. Results show that generally the three immersion joints have a more significant joint opening range than most dilation joints, with the exception of D11 which exhibits the most significant deformation (-5.18 to −0.26 mm). Compared with the three immersion joints and dilation joint D11, the deformation range of the other nine dilation joints is significantly lower (between −2.0 mm to + 1.0 mm).

It should be pointed out that the local peak opening of joints I2 and I3 on February 18 was recorded after a two-week break in the monitoring. As seen in Fig. 11, the coldest period of the year occurred over these two weeks. This cold episode lasted from around February 7 to 16, with the lowest mean temperature reaching −9 °C in the Heinenoord region on February 16 (Meteoblue [14]). Although on February 18 the temperature rose to a positive value (about 7 °C), the peak deformations at I2 and I3 indicate that the opening deformation curve exhibits a time delay when compared to the ambient temperature change. This deformation delay occurs in all resulting curves and will be analyzed in further detail below. As the temperature recovered to an above-zero level after February 18, the openings at I2 and I3 decreased rapidly during the following days.

Observing the whole year of monitoring, it is evident that the measured joint opening exhibits cyclical behavior. Specifically, the joint opening decreases (a joint gap closure) from spring to summer seasons, while in the summer period (June to September) the joint shows the maximum negative opening (namely the maximum joint gap closure); after September, the joint opening gradually increases during the colder period from October to December (an indication of joint gap opening). Note that this cyclic seasonal opening deformation is present at all instrumented joints.

Moreover, the degree of joint opening also varies according to joint location. Among the three immersion joints, the opening range (a difference between the highest and the lowest value) of I2 and I3 is higher than that of I1 (see Fig. 16), as I2, I3 and I1 have opening ranges of 6.15 mm, 5.73 mm and 3.21 mm, respectively. In addition, among the thirteen joints, D11 had the highest joint closure at −5.18 mm (on June 18, also with the highest measured temperature). It should be noted that during previous maintenance work, a significant leakage was observed at joint D11 [16]. This may indicate that D11 has higher deformation flexibility than the other nine dilation joints, which is consistent with the large joint opening measured by the DOFS system.

The monitoring result of joint I1 is analyzed in depth to investigate the potential correlation of seasonal temperature with joint deformation. Fig. 17 presents the measured temperature and joint deformation within the one-year period. Monitoring results show that the joint gap closes in warm seasons (summer period, with a maximum closure of around 2.84 mm), and opens in cold seasons (winter period, with a maximum opening of about 0.33 mm), and this cyclic deformation is related to the thermal expansion of the tunnel segment body. Within one year, the scale of joint uneven settlement (between −1.28 mm to 0.7 mm) is smaller than that of opening (between −2.84 mm to 0.33 m), and uneven settlement is measured to show seasonal variation as well. The joint deformation shows a correlation with temperature, which will be

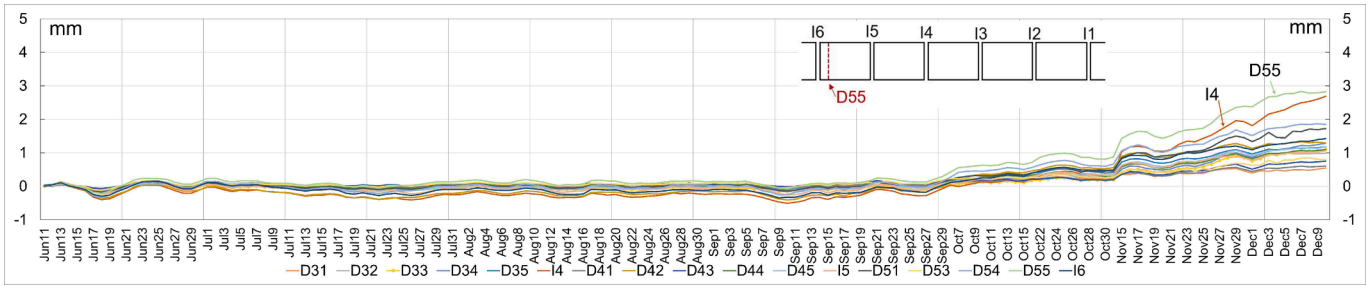


**Fig. 18.** Measured opening of second-set 17 joints (half-year period).

**Table 2**
Joint opening deformation range (unit:mm).

| | I1 | D11 | D12 | D13 | D14 | D15 | I2 | D21 | D22 | D23 | D24 | D25 | I3 |
|---|---|---|---|---|---|---|---|---|---|---|---|---|---|
| Min | −2.84 | −5.18 | −1.60 | −1.72 | −1.34 | −1.65 | −3.42 | −1.06 | −1.01 | −1.47 | −1.71 | −1.18 | −3.22 |
| Max | 0.37 | −0.26 | −0.08 | 0.05 | 0.24 | 0.14 | 2.72 | 0.08 | 0.02 | 0.18 | 0.07 | −0.04 | 2.51 |
| Amplitude | 3.21 | 4.92 | 1.53 | 1.77 | 1.59 | 1.79 | 6.15 | 1.14 | 1.03 | 1.65 | 1.78 | 1.14 | 5.73 |

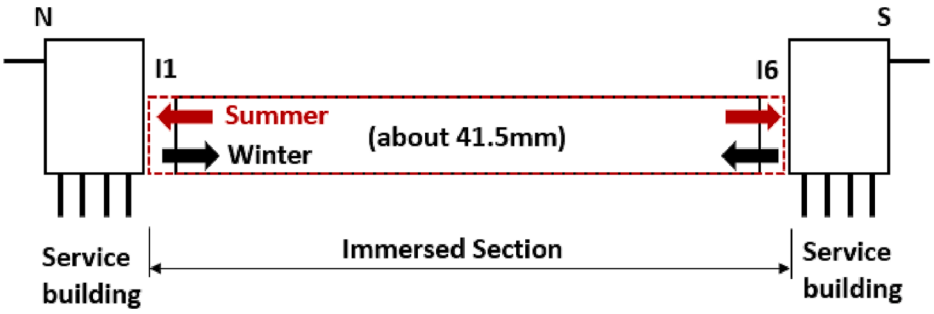


**Fig. 19.** Longitudinal expansion and contraction deformation of Heinenoordtunnel.

discussed more in further section 3.3. Also, there exists a delay between joint opening deformation and temperature change, indicating the joint opening is delayed after the temperature change. At joint I1 (and also most of the other joints), this delay is measured to be about 1 to 2 days; this delay phenomenon is more significant when strong temperature fluctuations occur, for instance from March 29 to April 3 in Fig. 17.

Fig. 18 shows the measured opening of the second-set seventeen joints (from D31 to I6) during a half-year period (June 11 to December 10, 2021). During the summer period (June to September), the joint opening remains relatively steady within the range of −0.5 mm to 0.5 mm. Nonetheless, when the ambient temperature gradually falls from October onwards, tunnel segment shrinkage results in a gradually increasing joint opening. D55 and I4 exhibit the most significant deformation of the seventeen joints, with a maximum opening of 2.80 mm and 2.69 mm, respectively, by December 10, 2021, while at other joints the maximum joint opening is below 2.0 mm. The measurement results validate that cyclic seasonal joint opening also occurs on the second set of instrumented joints.

The range of joint openings throughout the monitoring period is listed in Table 2 and Table A.1 in Appendix A. From the results, it can be seen that generally the opening deformation amplitude of immersion joints is larger than that of dilation joints. However, at a few dilation joints (D11, D54 and D55), a larger joint opening occurs compared with that at the nearby immersion joint. D11 exhibits the most significant opening, with a maximum of about −5.18 mm. As such, the monitoring results by DOFS system have properly revealed the magnitude of seasonal joint opening deformation, which can help to analyze seasonal tunnel behaviors.

Based on the thermal behavior of concrete segments, the seasonal joint opening deformation is closely related to the thermal expansion of the segment body longitudinally. For instance, the maximum joint closure occurs in summer period, when the segment expansion causes a narrowed joint gap. Specifically, in summer the segment expansion narrows the joint gap (resulting in a joint closure), and in winter the segment shrinkage widens the joint gap (a resultant joint opening). The measurements results help to quantitatively assess the scale of longitudinal thermal expansion of the full immersed section. Here the total joint opening of all the measured joints is summed up as in Eq. (11):

$$\Delta L = \sum \Delta y_i \tag{11}$$

where $\Delta L$ is the longitudinal thermal deformation of the full immersed section (about 574 m), and $\Delta y_i$ indicates the measured joint opening at joint $i$.

Considering a total of thirty joints over a half-year period (baseline on June 11, 2021), the total opening is calculated as 0.12 m on June 11 and 41.67 mm on December 10, 2021. This indicates throughout the half-year course (from summer to winter), the overall thermal shrinkage deformation of the 574 m immersed section is approximately 41.5 mm, as seen in Fig. 19. Moreover, the theoretical thermal expansion of this entire immersed section is calculated to be around 62 mm within this half-year period (with an expansion coefficient of 6E-6 per ℃ and a temperature change of 18℃), which is on the same scale as the measurement. Therefore, based on measurement results, the entire immersed section exhibits a cyclic thermal expansion and contraction with an amplitude of around 41.5 mm over the monitoring year, and this longitudinal thermal deformation is primarily compensated by joint opening variation(especially at the immersion joints).

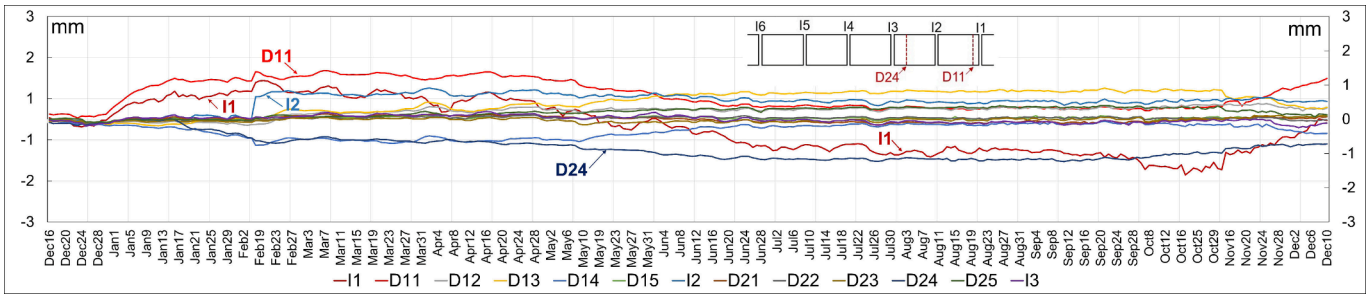


**Fig. 20.** Measured uneven settlement of 13 joints (full-year period).

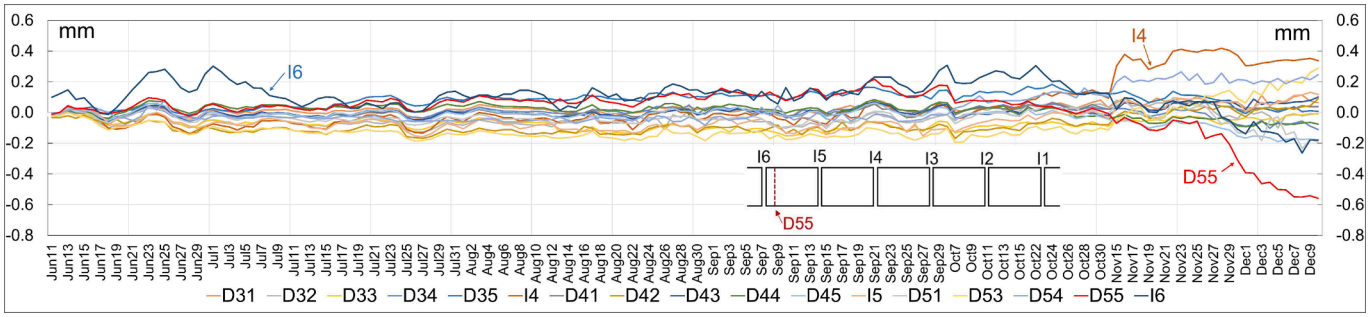


**Fig. 21.** Measured uneven settlement of second set 17 joints.

**Table 3**
Range of joint uneven settlement (unit:mm).

| | I1 | D11 | D12 | D13 | D14 | D15 | I2 | D21 | D22 | D23 | D24 | D25 | I3 |
|---|---|---|---|---|---|---|---|---|---|---|---|---|---|
| Min | −1.36 | 0.03 | −0.15 | −0.16 | −0.63 | −0.12 | −0.11 | −0.14 | −0.11 | −0.14 | −1.03 | −0.07 | −0.25 |
| Max | 0.94 | 1.18 | 0.38 | 0.76 | −0.05 | 0.10 | 0.76 | 0.13 | 0.10 | 0.10 | 0.01 | 0.33 | 0.23 |
| Amplitude | 2.30 | 1.15 | 0.53 | 0.92 | 0.58 | 0.22 | 0.88 | 0.27 | 0.21 | 0.24 | 1.05 | 0.41 | 0.48 |

### 3.2.2. *Joint uneven settlement*

Figs. 20 to 21 show the joint uneven settlement results of the first set of thirteen joints (full-year period, from December 16, 2020, to December 10, 2021) and the second set of seventeen joints (half-year period, from June 11, 2021, to December 10, 2021).

In the majority of the thirteen joints in a full-year period, joint uneven settlement is small (with an absolute value below 1.5 mm). Except for joints I1, D11 and D24, the uneven settlement of all joints falls within a range of −1.0 m to 1.0 mm (more specifically, the majority of joints only have a deformation range of −0.3 mm to 0.5 mm). However, D11 exhibits a maximum uneven settlement of about 1.3 mm, while I1 has a maximum (negative) deformation of around −1.4 mm.

Joint uneven settlement over a full-year period shows a seasonal variation as well. As shown in Fig. 20, for instance the uneven settlement of joint I1 increases from December 2020 to March 2021, then it decreases gradually from April until November 2021, and afterward it recovers to about 0.0 mm by December 2021, demonstrating a cyclic behavior. Nonetheless, the seasonal variation behavior of uneven settlement is not as significant as that of joint opening, and this will be explored in further detail in section 3.3. At joint I2, the deformation curve reaches a peak value in February (on February 18). This local peak is a result of the unusually low temperatures during the two-week break, as also shown in the opening result measurement in Fig. 16. Afterward, this deformation gradually decreases with time.

When comparing uneven settlement with opening, it can be seen that the scale of opening is generally much larger than that of uneven settlement, as shown in Tables 2 and 3. At D11, for example, the joint opening ranges from −5.18 to −0.26 mm, while the range of uneven settlement is only from 0.03 to 1.18 mm.

Fig. 21 shows the measured uneven settlement of second-set seventeen joints over a half-year period. It can be seen that most joints exhibit a fairly minor deformation range (-0.3 mm to + 0.4 mm) within this monitoring period, but joint D55 exhibits a larger deformation (about −0.6 mm by December 10) during the winter period.

During the summer months (June to September, with reasonably steady temperatures), the uneven settlement is very stable and within a limited range of −0.2 mm to 0.2 mm for the majority of joints (excluding I6). However, from November when the temperature fluctuates more significantly, the uneven settlement starts to show significant fluctuations also. For example, as demonstrated in Fig. 21, at I4 and D55 the fluctuation is more significant than at the other fifteen joints.

The amplitudes of joint uneven settlement are reported in Table 3 and Table A.1 in Appendix A. Generally, the scale of uneven settlement is significantly smaller than that of opening. For the first set of thirteen joints over an entire year, the deformation amplitude of most joints is below 1.0 mm, while I1 and D11 show a significantly larger deformation range, especially at joint I1. The measurement result shows the uneven settlement of some joints also exhibits cyclic seasonal behavior, and the discussion on its correlation to temperature will be in section 3.3.

Joint uneven settlement helps to illustrate the vertical plane deformation of an immersed tunnel. Here, the cumulated joint uneven settlement along the longitudinal axis of the tunnel is calculated using Eq. (12):

$$\Delta S_k = \sum_i^k \Delta z_i \tag{12}$$

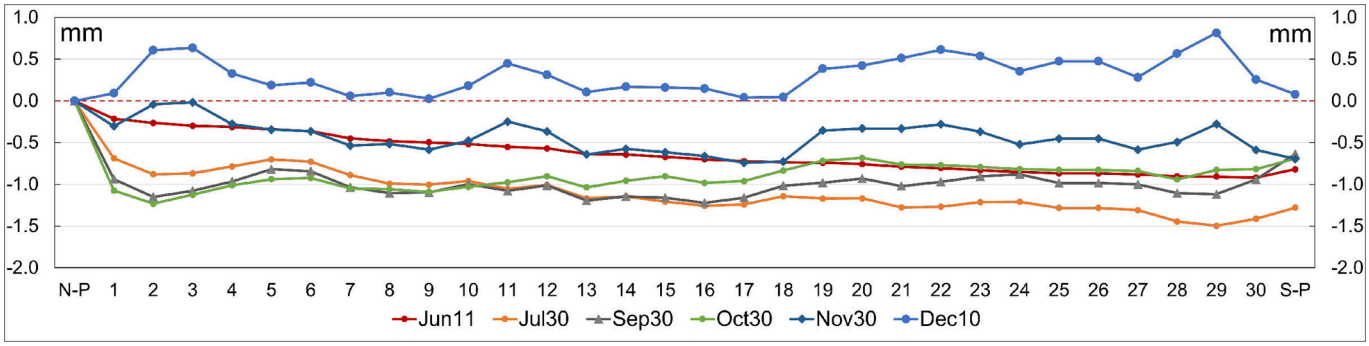


**Fig. 22.** Cumulated uneven settlement along the longitudinal tunnel axis.

**Table 4**
Correlation of joint deformation with temperature (I1 to I3).

| Joint | I1 | D11 | D12 | D13 | D14 | D15 | I2 | D21 | D22 | D23 | D24 | D25 | I3 |
|---|---|---|---|---|---|---|---|---|---|---|---|---|---|
| $C_{ot}$ | −0.93 | −0.89 | −0.92 | −0.92 | −0.95 | −0.94 | −0.85 | −0.96 | −0.97 | −0.93 | −0.93 | −0.97 | −0.89 |
| $C_{st}$ | −0.67 | −0.70 | 0.38 | 0.79 | 0.55 | −0.05 | 0.12 | −0.75 | 0.32 | −0.35 | −0.79 | 0.80 | −0.44 |

Note: $C_{ot}$ and $C_{st}$ mean opening-temperature correlation and uneven settlement-temperature correlation.

where $\Delta S_k$ is the cumulated joint uneven settlement at the *kth* joint (from the north), and $\Delta z_i$ indicates the uneven settlement at individual joint *i*(between the first and the *kth* joint).

Fig. 22 plots the accumulated joint uneven settlement on some selected days (N-P and S-P mean north and south portals). Here the settlement is set as relative to the north portal, and it can be seen that the calculated settlement of the south portal is not equal to zero. Considering the southern tunnel entrance ramp and service building have exhibited negligible settlements over time [17] and can be considered a fixed point, the measured uneven settlement implies segment tilting exists in the vertical plane. Furthermore, because the cumulative settlement curves show seasonal fluctuations, this may suggest that segment tilting also exhibits a seasonal variation. For a specific tilting behavior analysis, additional information, such as the tilting angle of each segment, should be monitored in addition to the joint uneven settlement data provided by the DOFS system.

### 3.3. Correlation of joint deformation with temperature

In this section, the joint deformations and temperature data are explicitly compared to investigate the potential correlation. The Pearson correlation coefficient between joint opening and uneven settlement on one hand, and temperature on the other hand are obtained. The coefficient results of the first set thirteen joints (I1 to I3, full-year period) are shown in Table 4, while those of the remaining seventeen joints (half-year period) are provided in Table A.2 in Appendix A.

As demonstrated in Table 4 and Table A.2, the opening at all joints has a strong negative correlation to temperature, with all values above −0.85 (most are above −0.90). The significant negative correlation strongly implies that the joint gap tends to widen with decreasing temperature (winter period) and close with increasing temperature (summer period). As described in section 3.2, the joint opening variation during seasonal temperature changes is strongly connected to the longitudinal thermal expansion of the tunnel segments (see Fig. 2).

Compared with joint openings, the correlation between uneven settlement and temperature varies significantly between joints. This implies the relationship between uneven settlement and temperature is generally much weaker than that between opening and temperature. In addition, it should be mentioned that the temperature effects on the sensing fiber may amplify any system errors, since most joints present only a very low uneven settlement amplitude, far below 1 mm, over the one-year or half-year period. Observing the deformation range of joint opening and uneven settlement, it is reasonable to conclude that for a long segmented immersed tunnel the seasonal temperature change will cause a much more significant deformation reaction longitudinally than in the vertical direction.

## 4. Assessing the impacts of seasonal joint deformations

The seasonal joint deformations may impact the tunnel safety and should be assessed to provide feedbacks for regular tunnel maintenance. According to the monitoring results by the DOFS system, in the Heinenoordtunnel only joints I1 and D11 show a slightly more significant seasonal uneven settlement, with amplitudes of 2.30 mm and 1.15 mm respectively. At all other joints this seasonal uneven settlement remains at a small sub-millimeter scale, and such low or even negligible uneven settlement generally imposes limited impacts for the tunnel structural safety. However, the seasonal joint opening range is much more significant (with a scale of several millimeters), and its potential impacts on the tunnel joint performance should be investigated.

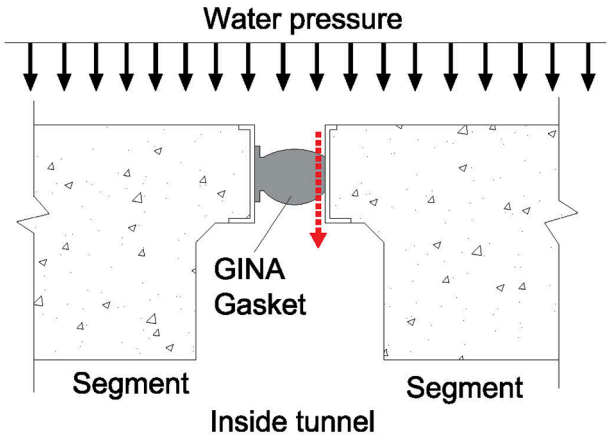


**Fig. 23.** Potential leakage risk due to large joint opening.

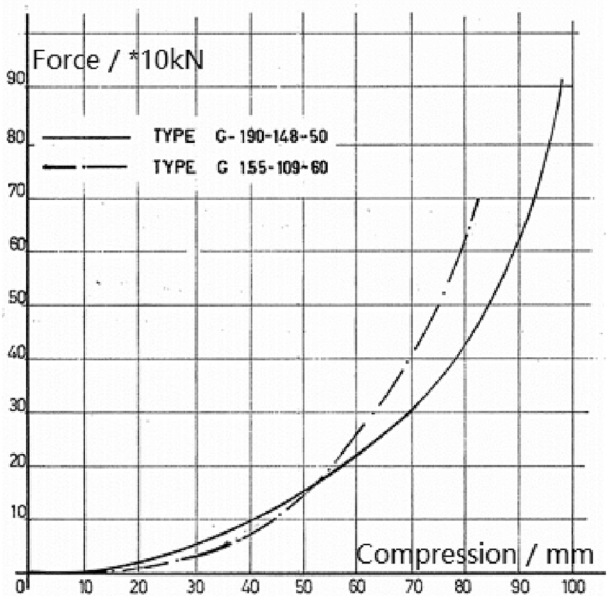


**Fig. 24.** Compression behavior of GINA gasket.

### 4.1. Immersion joint

(1). GINA compression status analysis.

At the immersion joints, the sealing performance of the GINA gasket is determined by its compression state, as shown in Fig. 23, and large joint opening would lead to decompression of the gasket, which may increase the leakage risk at these joints. During the tunnel construction stage, a tunnel element is immersed and connected to the already

**Table 5**
Compression status examination of GINA gasket.

| Joint | I1 | I2 | I3 | I4 | I6 |
|---|---|---|---|---|---|
| Depth (section-middle, m) | 7.19 | 12.44 | 17.02 | 17.02 | 7.16 |
| Hydrostatic force (kN) | 32,187 | 44,037 | 44,037 | 32,161 | 32,161 |
| Force per meter (kN) | 418 | 572 | 572 | 418 | 418 |
| GINA type | G109 | G148 | G148 | G148 | G109 |
| Initial compression (mm) | 70 | 87 | 87 | 79 | 70 |
| Opening amplitude (mm) | 3.2 | 6.2 | 5.7 | 3.2 | 1.8 |
| Minimum compression (mm) | 66.7 | 81.8 | 81.3 | 75.8 | 68.2 |
| Maximum compression (mm) | 73.2 | 93.2 | 92.7 | 82.2 | 71.8 |

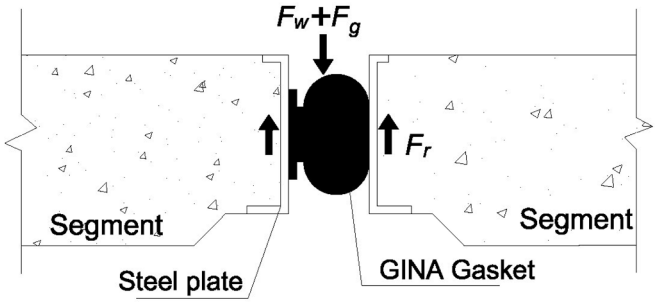


**Fig. 25.** Force Equilibrium on GINA gasket at immersion joint.

finished one under the river, and the GINA gasket installed on one element end is compressed by the water-pressure on the other end, while the degree of this compression is determined by the depth of element under water. In the Heinenoordtunnel, two types of GINA gasket are used, namely G-190–148-50 and G-155–109-60 [21]. Type G-155–109-60 gasket has a lower compression limit and was used in the first and last immersion joints (I1 and I6, see Fig. 12), while Type G-190–148-50 has larger dimensions and is used at the other three immersion joints (the 2nd, 3rd and the 4th joints from north). Note that the 5th immersion joint was constructed by on-site concreting and has a different behavior compared with other normal immersion joints with GINA gaskets.

The compression curve (force-compression) of the two GINA gasket types is shown in Fig. 24. The depth of each joint, the hydrostatic pressure, and the initial compression of the GINA gasket at specific joints are computed and reported in Table 5, based on the longitudinal alignment of the Heinenoordtunnel. Here, the initial compression of the GINA is set as the baseline, and the maximum compression over the monitoring period is calculated by adding the measured joint opening amplitude (to the baseline), while the minimum compression is obtained by subtracting the seasonal opening amplitude (from the baseline), as demonstrated in Table 5.

(2). **Watertightness evaluation of immersion joints**.

The effects of seasonal opening on the watertightness of the immersion joint are assessed subsequently. Considering the equilibrium between the forces on the GINA profile in Fig. 25, it was assumed that when the external water pressures and soil weight push the GINA gasket inwardly, a leakage risk occurs. To prevent this GINA displacement, friction forces on the GINA-segment interface must resist such external pressures on the GINA profile[21], as shown in Eq. (13):

$$F_w + F_g \leq F_r \tag{13}$$

Where $F_w$ and $F_g$ refer to the external water pressure force and ground soil force respectively, while $F_r$ means the interface friction force (two sides), which can be computed by multiplying the GINA compression force by the friction coefficient between rubber and steel frame (here 0.6 is taken according to Van Montfort [21]. Note that this force equilibrium corresponds to an extreme scenario where the bolt

**Table 6**
Immersion joint watertightness evaluation parameters.

| Joint | I1 | I2 | I3 | I4 | I6 |
|---|---|---|---|---|---|
| GINA type | G109 | G148 | G148 | G148 | G109 |
| Depth (section-top, m) | 2.89 | 8.14 | 12.72 | 12.72 | 2.86 |
| $F_w$(kN) | 14 | 40 | 62 | 62 | 14 |
| $F_g$(kN) | 15 | 20 | 20 | 20 | 15 |
| Total external force (kN) | 29 | 60 | 82 | 82 | 29 |
| Initial GINA force (kN) | 418 | 572 | 572 | 418 | 418 |
| Minimum GINA force (kN) | 350 | 460 | 465 | 375 | 380 |
| Minimum force after relaxation (kN) | 194 | 255 | 258 | 208 | 211 |
| Total friction force (kN) | 233 | 306 | 309 | 249 | 253 |

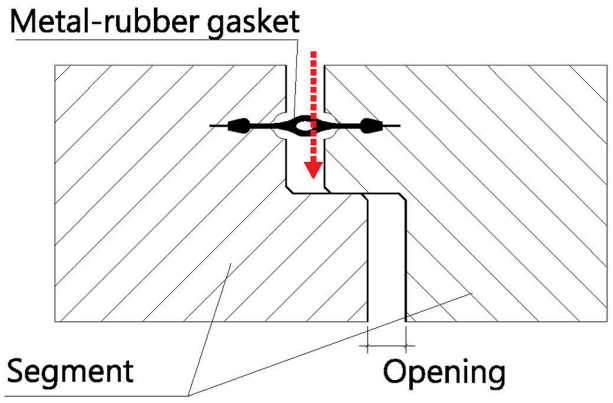


**Fig. 26.** Leakage at dilation joint due to excessive opening.

fixture resistance entirely vanishes due to complete bolt corrosion.

It should be noted that the rubber used for GINA gaskets shows some relaxation with time, resulting in decreased compression force at the gasket. The Heinenoordtunnel was constructed in 1969; hence the relaxation must be determined over a period of 52 years (with 365 days per year). According to the gasket property sheet provided by the manufacturer [21], the relaxation index $R$ is calculated as in Eq. (14):

$$R = 0.06^{*}log(t) \tag{14}$$

Where $t$ is the cumulated relaxation time duration (by second).

Since the opening of the tunnel, it is estimated that the GINA rubber has relaxed by 44.6%, meaning that only 55.4% of the original compression force remains on the contact face. The force due to the weight of the soil depends on the volumetric weight of the soil and the height of the soil column above the joint. The unit weight of the soil above the joint is set as 10 kN/m$^3$, and above joints I1 and I6, a soil cover of 2 m is assumed, while on the other joints the cover is 4 m thick.

For the worst-case scenario, when the minimum compression occurs at each joint, the watertightness evaluation results are specified in Table 6. From the results it can be observed that the overall external forces on the GINA gasket are far less than the total friction forces, indicating that under normal operational conditions, the seasonal joint expansion generally imposes quite limited effects on joint watertightness.

It should be noted, however, that the watertightness evaluation is based on normal working conditions, and the compression state of the GINA gasket is only evaluated considering the first construction stage. In this study, the evaluation procedure is improved by assessing the current compression state during service and the condition of the gasket fixing bolts. In some cases, for instance, the opening at particular locations of the joint cross-section (for example, at joint roof or floor) may be even larger than the measured values by the DOFS system, indicating that tunnel managers will need to be aware of the possibility of excess joint decompression.

### 4.2. Dilation joint

At the dilation joints, an embedded metal-rubber gasket is used as a seal, as shown in Fig. 1(b). Generally this integrated gasket can withstand a limited extension before rupture, and this limit is estimated to be 35 mm in the Heinenoordtunnel by Rijkswaterstaat [16]. However, a 15 mm tensional deformation may still cause a leakage. If the joint opening is too large, the metal-rubber gasket may be over-tensioned, which increases the chance of leaking, as shown in Fig. 26. According to the measurement by the DOFS system, most dilation joints have an opening range of less than 2 mm, which implies a minor influence on joint watertightness.

However, at three dilation joints, namely D11(4.92 mm), D54(2.20 mm) and D55(3.02 mm), the opening amplitude is significantly higher than that of the others. Notably, these three joints are in close proximity to the two side portals of the immersed tunnel, and tend to exhibit higher deformation flexibility than the rest dilation joints. Moreover, during previous Heinenoordtunnel maintenance procedures, serious leakages were observed at joints D11 and D54, necessitating a significant injection repair work. This suggests that there may have been excessive joint deformation at these points, which is consistent with field measurements. In Heinenoordtunnel maintenance, the dilation joints adjoining the two approach portals warrant more attention, and the joint opening of these zones should be examined more frequently before major leakage occurs.

## 5. Conclusions

This study investigates the seasonal deformations of an immersed tunnel based on actual field monitoring, and assesses their impact on tunnel structural safety. The research work starts with the design of an innovative distributed optical fiber sensor (DOFS) system and implements it to monitor the seasonal joint deformations of the Heinenoordtunnel in the Netherlands. This developed DOFS system measures both joint opening and uneven settlement of immersion and dilation joints, and monitoring results over one-year period are presented.

The main conclusions in this study are:

(1). The distributed optical fiber sensor (DOFS) is an effective sensing technique to monitor seasonal joint deformations (of both dilation and immersion joints) in an immersed tunnel. The system proves capable to measure the opening and uneven settlement with better than millimeter accuracy.
(2). Seasonal periodic joint opening occurs at the tunnel joints, and this joint opening shows a negative correlation with temperature, indicating that the joint gap tends to close during summer and open during winter.
(3). The amplitudes of seasonal opening at immersion joints (with a range of 1.77 to 6.15 mm) are larger than those of most dilation joints (which fall within a range of 0.6 mm to 2.0 mm). However, for a few dilation joints the deformations are still significant, implying that dilation joints should be given the same consideration as immersion joints in a rational tunnel monitoring plan.
(4). The joints at two end sections very close to the approach structure exhibit a more significant opening deformation, indicating a higher degree of flexibility. In addition, a delay (in the order of 1 to 2 days) exists between temperature change and joint opening, which suggests that joint opening is delayed with respect to the ambient temperature change.
(5). For most joints, the amplitude of uneven settlement is less than 1 mm, and this magnitude of uneven settlement is significantly smaller than that of joint opening. Moreover, the joint uneven settlement also exhibits a seasonal variation, but its correlation to temperature is significantly weaker than that of joint opening.
(6). Based on analysis of field monitoring results, seasonal joint opening generally imposes a limited impact on the structural

**Table A1**
Measured joint deformation range (D31 to I6).

| | | D31 | D32 | D33 | D34 | D35 | I4 | D41 | D42 | D43 | D44 | D45 | I5 | D51 | D53 | D54 | D55 | I6 |
|---|---|---|---|---|---|---|---|---|---|---|---|---|---|---|---|---|---|---|
| Opening | Min | −0.07 | −0.17 | −0.16 | −0.15 | −0.20 | −0.50 | −0.06 | −0.40 | −0.08 | −0.18 | −0.19 | −0.26 | −0.18 | −0.11 | −0.34 | −0.21 | −0.35 |
| | Max | 0.55 | 1.01 | 1.10 | 1.29 | 1.17 | 2.69 | 0.61 | 1.33 | 0.75 | 1.09 | 1.17 | 1.06 | 1.72 | 0.85 | 1.87 | 2.83 | 1.43 |
| | Amplitude | 0.62 | 1.18 | 1.26 | 1.44 | 1.37 | 3.19 | 0.67 | 1.73 | 0.83 | 1.27 | 1.36 | 1.32 | 1.91 | 0.96 | 2.20 | 3.04 | 1.77 |
| Settlement | Min | −0.05 | −0.13 | −0.15 | −0.11 | −0.02 | −0.14 | −0.06 | −0.17 | −0.06 | −0.09 | −0.19 | −0.16 | −0.24 | −0.19 | −0.08 | −0.56 | −0.26 |
| | Max | 0.11 | 0.08 | 0.00 | 0.07 | 0.18 | 0.42 | 0.07 | 0.09 | 0.10 | 0.08 | 0.06 | 0.13 | 0.10 | 0.29 | 0.26 | 0.22 | 0.31 |
| | Amplitude | 0.16 | 0.21 | 0.16 | 0.18 | 0.20 | 0.55 | 0.12 | 0.26 | 0.16 | 0.18 | 0.25 | 0.29 | 0.33 | 0.48 | 0.35 | 0.78 | 0.57 |

integrity and joint watertightness. However, at the dilation joints adjoining the two approach ramps, the monitored large deformation shows a substantial opening and suggests a possibly deteriorated structural integrity. Therefore, during tunnel maintenance, these problematic dilation joints should be further examined for safety concerns.

## CRediT authorship contribution statement

**Xuehui Zhang:** Conceptualization, Methodology, Investigation, Writing – original draft. **Wout Broere:** Supervision, Funding acquisition, Conceptualization, Writing – review & editing.

## Declaration of Competing Interest

The authors declare that they have no known competing financial interests or personal relationships that could have appeared to influence the work reported in this paper.

## Data availability

Data will be made available on request.

## Acknowledgements

This research has been financially supported by China Scholarship Council (China) and Rijkswaterstaat, the Netherlands and European Union's Horizon 2020 Research and Innovation Programme (Project SAFE-10-T under Grant No. 723254). The authors thank Rijkswaterstaat for granting the access to the tunnel and the installation of the sensors.

## Appendix A

(See Tables A1-A2).

**Table A2**
Correlation of joint deformation with temperature (joint D31 to I6).

| Joint | D31 | D32 | D33 | D34 | D35 | I4 | D41 | D42 | D43 | D44 | D45 | I5 | D51 | D53 | D54 | D55 | I6 |
|---|---|---|---|---|---|---|---|---|---|---|---|---|---|---|---|---|---|
| $C_{ot}$ | −0.99 | −0.96 | −0.92 | −0.94 | −0.96 | −0.90 | −0.97 | −0.95 | −0.96 | −0.96 | −0.96 | −0.97 | −0.94 | −0.96 | −0.94 | −0.87 | −0.95 |
| $C_{st}$ | −0.86 | −0.72 | −0.46 | 0.15 | −0.12 | −0.92 | −0.83 | −0.82 | −0.84 | 0.59 | 0.61 | −0.82 | −0.06 | −0.82 | −0.88 | 0.55 | 0.32 |

## References

[1] B.J. Berkhout, et al. 2014. Instandhouding zinkvoegen. Technical report T330, COB, Delft, The Netherlands. https://www.cob.nl/document/instandhouding-zinkvoegen/.
[2] Y. Bai, H. Lu, Damage analysis and repair technology of OMEGA gasket in immersed tube tunnel, J. Railway Eng. Soc. 9 (2016) 87–92 (In Chinese).
[3] W. Broere, K. de Haas, B. Berkhout, H.R.E. Dekker, 2022, Managing knowledge for future-proof tunnels in the Netherlands, ITA WTC Copenhagen, 2022.
[4] Fibristerre (2021), Information of BOFDA interrogator see https://www.fibristerre.de/files/fibrisTerre_flyer.pdf (latest accessed in June 2021).
[5] K.G. Gavin, W. Broere, M.S. Kovačević, K. de Haas, Investigation of the remaining life of an immersed tube tunnel in The Netherlands, in: In *Proceedings of the WTC 2019 ITA-AITES World Tunnel Congress*, 2019, p. 4831.
[6] T. Horiguchi, K. Shimizu, T. Kurashima, M. Tateda, Y. Koyamada, Development of a distributed sensing technique using Brillouin scattering, J. Lightwave Technol. 13 (1995) 1296, https://doi.org/10.1109/50.400684.
[7] R. Lunniss, J. Baber, Immersed tunnels, CRC Press, 2013.
[8] J.M. López-Higuera, L.R. Cobo, A.Q. Incera, A. Cobo, Fiber optic sensors in structural health monitoring, J. lightwave technol. 29 (4) (2011) 587–608.
[9] W. Li, D. Wu, X. Guo, X. Gao, Overhaul design and construction of ningbo yongjiang immersed tube tunnel, Modern Tunn. Technol. 48 (1) (2011) 81–89. In Chinese.
[10] H. Li, H. Zhu, et al., Experimental investigation on pipe-soil interaction due to ground subsidence via high-resolution fiber optic sensing, Tunn. Undergr. Space Technol. 127 (2022), 104586.
[11] Limfjord Tunnel report, 2019. Limfjord Tunnel Assessment and Retrofitting Technical Summary Report, Version 1.0., see https://www.trm.dk/media/tdxldt25/teknisk-rapport-limfjord.pdf (lateast accessed in April, 2022).
[12] A. Motil, A. Bergman, M. Tur, State of the art of brillouin fiber-optic distributed sensing, Opt. Laser Technol. 78 (2016) 81–103.
[13] H. Mohamad, K. Soga, et al., Monitoring twin tunnel interaction using distributed optical fiber strain measurements, J. Geotech. Geoenviron. Eng. 138 (8) (2012) 957–967.
[14] Meteoblue weather report information, latest accessed in March, 2022. https://www.meteoblue.com/en/weather/historyclimate/weatherarchive/heinenoord_netherlands_2754507?fcstlength=1m&year=2021&month=1.
[15] H. Ohno, H. Naruse, M. Kihara, A. Shimada, Industrial applications of the BOTDR optical fiber strain sensor, Opt. Fiber Technol. 7 (1) (2001) 45–64.
[16] Rijkswaterstaat, Report-Lekkage-in-tunnels-dilatatievoegen-beton, 2008.

[17] Rijkswaterstaat GPO. 2016. Report-Deformatiemeting-37H-312-01.
[18] Rijkswaterstaat. 2022. Photography of Heinenoordtunnel at Rijkswaterstaat website, Netherlands. (https://www.rijkswaterstaat.nl).
[19] R. Rahadian, S. van der Woude, D. Wilschut, C.B. Blom, W. Broere, A new test setup for studying sand behaviour inside an immersed tunnel joint gap. InPhysical Modelling in Geotechnics, CRC Press, 2018, pp. 443–448.
[20] Y. Sui, X. Cheng, et al., Distributed fibre optic monitoring of damaged lining in double-arch tunnel and analysis of its deformation mode, Tunn. Undergr. Space Technol. 110 (2021), 103812.
[21] R. Van Montfort, Insufficiency of immersion joints in existing immersed tunnels: Case study on functioning of Gina-seal and Omega-seal in the Kil Tunnel, Delft University of Technology, Delft, The Netherlands, 2018. MSc Thesis.
[22] X. Wang, B. Shi, G. Wei, S. Chen, H. Zhu, T. Wang, Monitoring the behavior of segment joints in a shield tunnel using distributed fiber optic sensors, Struct. Control Health Monit. 25 (2018) e2056.
[23] S. Wang, X. Zhang, Y. Bai, Comparative study on foundation treatment methods of immersed tunnels in China, Front. Struct. Civ. Eng. 14 (1) (2020) 82–93.
[24] H. Zhu, D. Wang, B. Shi, X. Wang, G. Wei, Performance monitoring of a curved shield tunnel during adjacent excavations using a fiber optic nervous sensing system, Tunn. Undergr. Space Technol. 124 (2022), 104483.
[25] D. Wang, H. Zhu, J. Huang, Z. Yan, X. Zheng, B. Shi, Fiber optic sensing and performance evaluation of a water conveyance tunnel with composite linings under super-high internal pressures, J. Rock Mech. Geotech. Eng. 15 (10) (2023).
[26] X. Zhang, W. Broere, Sensing fiber selection for point displacement measuring with distributed optic fiber sensor, Measurement 197 (2022), 111275.
[27] X. Zhang, W. Broere, Design of a distributed optical fiber sensor system for measuring immersed tunnel joint deformations, Tunn. Undergr. Space Technol. 131 (2023), 104770.
[28] X. Zhang, W. Broere, Monitoring of tidal variation and temperature change induced movements of an immersed tunnel using Distributed Optical Fiber Sensor (DOFS), Struct. Control Health Monit. (2023) (accepted).